RESEARCH BRIEF

Diverse and Targetable Kinase Alterations Drive Histiocytic Neoplasms

Eli L. Diamond[1], Benjamin H. Durham[2], Julien Haroche[3], Zhan Yao[4], Jing Ma[5], Sameer A. Parikh[6], Zhaoming Wang[7], John Choi[5], Eunhee Kim[8], Fleur Cohen-Aubart[3], Stanley Chun-Wei Lee[8], Yijun Gao[4], Jean-Baptiste Micol[8], Patrick Campbell[9], Michael P. Walsh[5], Brooke Sylvester[8], Igor Dolgalev[10], Olga Aminova[10], Adriana Heguy[10], Paul Zappile[10], Joy Nakitandwe[5], Chezi Ganzel[11], James D. Dalton[5], David W. Ellison[5], Juvianee Estrada-Veras[12], Mario Lacouture[13], William A. Gahl[12], Philip J. Stephens[14], Vincent A. Miller[14], Jeffrey S. Ross[14], Siraj M. Ali[14], Samuel R. Briggs[1], Omotayo Fasan[15], Jared Block[16], Sebastien Héritier[17,18], Jean Donadieu[17,18], David B. Solit[8], David M. Hyman[19], José Baselga[19], Filip Janku[20], Barry S. Taylor[8], Christopher Y. Park[2,8], Zahir Amoura[3], Ahmet Dogan[2], Jean-Francois Emile[16,21], Neal Rosen[4], Tanja A. Gruber[5,9], and Omar Abdel-Wahab[8,22]

ABSTRACT

Histiocytic neoplasms are clonal, hematopoietic disorders characterized by an accumulation of abnormal, monocyte-derived dendritic cells or macrophages in Langerhans cell histiocytosis (LCH) and non-Langerhans cell histiocytosis (non-LCH), respectively. The discovery of *BRAF*^{V600E} mutations in approximately 50% of these patients provided the first molecular therapeutic target in histiocytosis. However, recurrent driving mutations in the majority of patients with *BRAF*^{V600E}–wild-type non-LCH are unknown, and recurrent cooperating mutations in non-MAP kinase pathways are undefined for the histiocytic neoplasms. Through combined whole-exome and transcriptome sequencing, we identified recurrent kinase fusions involving *BRAF, ALK*, and *NTRK1*, as well as recurrent, activating *MAP2K1* and *ARAF* mutations in patients with *BRAF*^{V600E}–wild-type non-LCH. In addition to MAP kinase pathway lesions, recurrently altered genes involving diverse cellular pathways were identified. Treatment of patients with *MAP2K1*- and *ARAF*-mutated non-LCH using MEK and RAF inhibitors, respectively, resulted in clinical efficacy, demonstrating the importance of detecting and targeting diverse kinase alterations in these disorders.

SIGNIFICANCE: We provide the first description of kinase fusions in systemic histiocytic neoplasms and activating *ARAF* and *MAP2K1* mutations in non-Langerhans histiocytic neoplasms. Refractory patients with *MAP2K1*- and *ARAF*-mutant histiocytoses had clinical responses to MEK inhibition and sorafenib, respectively, highlighting the importance of comprehensive genomic analysis of these disorders. *Cancer Discov; 6(2); 154–65. ©2015 AACR.*

[1]Department of Neurology, Memorial Sloan Kettering Cancer Center, New York, New York. [2]Department of Pathology, Memorial Sloan Kettering Cancer Center, New York, New York. [3]Internal Medicine Service, Hôpital Pitié-Salpêtrière, Paris, France. [4]Molecular Pharmacology and Chemistry Program, Memorial Sloan Kettering Cancer Center, New York, New York. [5]Department of Pathology, St. Jude Children's Research Hospital, Memphis, Tennessee. [6]Division of Hematology, Department of Medicine, Mayo Clinic, Rochester, Minnesota. [7]Department of Computational Biology, St. Jude Children's Research Hospital, Memphis, Tennessee. [8]Human Oncology and Pathogenesis Program, Memorial Sloan Kettering Cancer Center, New York, New York. [9]Department of Oncology, St. Jude Children's Research Hospital, Memphis, Tennessee. [10]Genome Technology Center, NYU Langone Medical Center, New York, New York. [11]Department of Hematology, Shaare Zedek Medical Center, Jerusalem, Israel. [12]National Human Genome Research Institute, National Institutes of Health, Bethesda, Maryland. [13]Dermatology Service, Department of Medicine, Memorial Sloan Kettering Cancer Center, New York, New York. [14]Foundation Medicine, Cambridge, Massachusetts. [15]Department of Hematologic Oncology and Blood Disorders, Levine Cancer Institute, Charlotte, North Carolina. [16]Hematopathology, Carolinas Pathology Group, Charlotte, North Carolina. [17]French Reference Center for Langerhans Cell Histiocytosis, Trousseau Hospital, Paris, France. [18]EA4340, Versailles University, Boulogne-Billancourt, France. [19]Developmental Therapeutics, Department of Medicine, Memorial Sloan Kettering Cancer Center, New York, New York. [20]Department of Medicine, The University of Texas MD Anderson Cancer Center, Houston, Texas. [21]Pathology Service, Hôpital universitaire Ambroise Paré, APHP, Boulogne, France. [22]Leukemia Service, Department of Medicine, Memorial Sloan Kettering Cancer Center, New York, New York.

Note: Supplementary data for this article are available at Cancer Discovery Online (http://cancerdiscovery.aacrjournals.org/).

E.L. Diamond, B.H. Durham, and J. Haroche contributed equally to this article and are listed alphabetically by last name.

Corresponding Author: Omar Abdel-Wahab, Zuckerman 802, Memorial Sloan Kettering Cancer Center, 802 Zuckerman Research Building, 415 East 68th Street, New York, NY 10065. Phone: 347-821-1769; Fax: 646-422-0856; E-mail: abdelwao@mskcc.org

doi: 10.1158/2159-8290.CD-15-0913

INTRODUCTION

Systemic histiocytic neoplasms consist of Langerhans cell histiocytosis (LCH) and the non-Langerhans forms of histiocytosis (non-LCH), including Erdheim–Chester disease (ECD), juvenile xanthogranuloma (JXG), and Rosai–Dorfman disease (RDD; ref. 1). These are diverse disorders marked by infiltration of tissues with neoplastic histiocytes whose cellular origins have long been debated. The discovery of the *BRAF*^{V600E} mutation in approximately 50% of patients with LCH (2, 3) and ECD (4) led to biologic and therapeutic advances in these disorders. For example, characterization of the cells in the hematopoietic system of patients with LCH at which the *BRAF*^{V600E} mutation arises resulted in the identification of LCH as derived from myelomonocytic precursors (3). Moreover, multiple reports have demonstrated that treatment of adult (5–7) and pediatric (8) patients with *BRAF*^{V600E}-mutant histiocytosis with vemurafenib (a RAF inhibitor that specifically targets *BRAF*^{V600E}) confers clinical responses in >90% of patients marked by a prolonged durability compared with that seen with BRAF inhibition in common *BRAF*^{V600E}-mutant malignancies. The robust efficacy of BRAF inhibitor therapy, especially in severe forms of non-LCH, stands in contrast to the relative ineffectiveness of existing treatments for adults with these disorders (9).

More recently, *MAP2K1* mutations have been identified in approximately 25% of patients with *BRAF*^{V600E}–wild-type LCH, reinforcing the notion that LCH is a disease driven by MAP kinase pathway activation (10–12). However, the direct clinical importance of activating *MAP2K1* mutations in LCH is unknown. Moreover, in contrast to LCH, activating kinase mutations in the majority of patients with *BRAF*^{V600E}–wild-type non-LCH are undefined. In addition, recurrent alterations that coexist with activating kinase mutations have not been defined for any of these conditions. Finally, despite the clinical and histopathologic differences between LCH and non-LCH, the molecular bases for these differences are not known.

To comprehensively define the genomic alterations in histiocytic neoplasms, we performed unbiased whole-exome and transcriptome sequencing across pediatric and adult LCH and non-LCH patients. In addition, on the basis of novel kinase alterations identified in this study, 3 patients with severe and refractory *BRAF*^{V600E}–wild-type non-LCH were successfully treated with targeted therapies, recapitulating the efficacy of BRAF inhibition in *BRAF*^{V600E}-mutated histiocytoses.

RESULTS

Whole-Exome and Transcriptome Sequencing across Histiocytic Neoplasms

To address the above, we performed whole-exome sequencing (WES) of frozen tumor biopsies from 24 patients with LCH (n = 10) or ECD (n = 14) paired with peripheral blood mononuclear cells. Thirteen of 24 patients also underwent RNA sequencing (RNA-seq; Supplementary Table S1). Both adult (n = 15; n = 2 with LCH) and pediatric cases (n = 9; n = 8 with LCH) were included. All mutations in activating kinases identified by WES or RNA-seq were validated by droplet-digital PCR (ddPCR), and all others were validated by targeted-capture next-generation sequencing (Supplementary Tables S2 and S3).

Overall, a mean of 7 nonsynonymous mutations per adult patient was identified (range, 1–22) compared with 5 mutations per pediatric patient (range, 4–9; P = ns; Supplementary Fig. S1). The median variant allele frequency (VAF) for the 23 individual known activating kinase mutations identified by WES was 11%, whereas the median VAF for all other somatic mutations was 10% (Supplementary Table S3). Combined WES and RNA-seq revealed mutations or fusions activating MAP kinase signaling in 100% of patients (Fig. 1A; Supplementary Fig. S2A and S2B). In addition, mutations affecting diverse biologic processes coexisted with activating kinase mutations, including recurrent mutations affecting the p38/MAPK and epigenetic regulatory pathways (Supplementary Table S3); however, inspection of the co-occurring genes demonstrated no clear differences in the frequencies of mutated specific genes or pathways of genes affected by mutations between the 24 LCH and non-LCH cases. An analysis of WES data from peripheral blood DNA used as the germline reference for pathologic mutations in a total of 565 cancer-associated genes (including 60 autosomal-dominant cancer predisposition genes, MAP kinase pathway members, as well as all genes reported as mutated in the recent studies of clonal hematopoiesis; refs. 13–15) failed to reveal mutations in any of these genes in blood DNA.

Recurrent *MAP2K1* and *ARAF* Mutations in Non-LCH Neoplasms

WES and RNA-seq revealed *MAP2K1* mutations in both LCH and non-LCH patients and *ARAF* mutations in non-LCH patients (Fig. 1; Supplementary Fig. S3A and S3B). Because neither *MAP2K1* nor *ARAF* mutations have previously been described in ECD, we next interrogated a validation cohort of 37 *BRAF*^{V600E}–wild-type, non-LCH, formalin-fixed, paraffin-embedded (FFPE) tissue cases (Fig. 1B). Exons 2 and 3 of *MAP2K1* and all coding regions of *ARAF* were sequenced, along with regions of recurrent mutations in *NRAS*, *KRAS*, and *PIK3CA*, because rare mutations in these genes have previously been noted in patients with *BRAF*^{V600E}–wild-type non-LCH (16). This revealed recurrent activating mutations in *MAP2K1* (32%; n = 12), *NRAS* (16%; n = 6), *KRAS* (11%; n = 4), *PIK3CA* (8%; n = 3), and *ARAF* (3%; n = 1; Fig. 1B–D). Expression of 10 of these *MAP2K1* mutants identified activation of MAP kinase signaling over wild-type MAP2K1 (Fig. 1E). Two non-LCH cases demonstrated concurrent activating *NRAS* and *ARAF* mutations. Eleven cases (30%; n = 11) did not demonstrate known activating mutations in these kinase genes based on targeted gDNA sequencing (Fig. 1A–D; Supplementary Figs. S2, S3C, and S3D).

Recurrent Kinase Fusions in Non-Langerhans Histiocytic Neoplasms

RNA-seq identified kinase fusions involving *BRAF*, as well as *ALK*, exclusively in *BRAF*^{V600E}–wild-type non-LCH (Fig. 1A; Supplementary Fig. S2). An *RNF11–BRAF* fusion was detected in an infiltrative, non-LCH brain lesion of a 14-year-old child (Fig. 2A; Supplementary Fig. S4A). Because kinase fusions have not been described in histiocytic neoplasms, we first confirmed

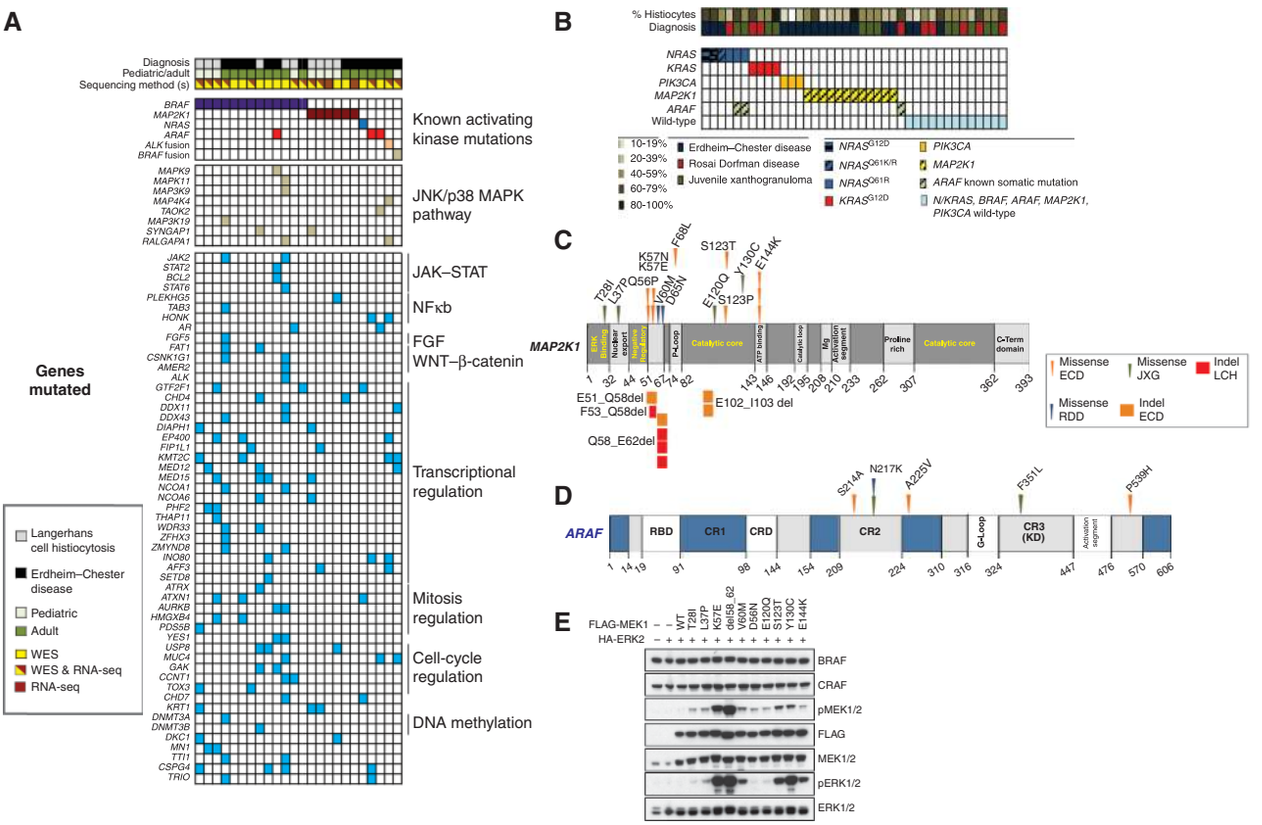

Figure 1. Mutational profiles of systemic histiocytic neoplasm patients and recurrent *MAP2K1* and *ARAF* mutations in non-Langerhans histiocytic neoplasms. **A,** results of whole exome and transcriptome sequencing of LCH and non-LCH neoplasms. Each patient is represented in one column. Diagnosis (LCH or ECD), age category, and sequencing method are in the first 3 rows. Somatic mutations identified are in the lower rows and subdivided based on mutations known to activate kinases, affect the JNK/p38 MAP kinase pathway, or involve a diverse array of co-occurring pathways (shown on the right). Only mutations identified in >1 sample and selected other mutations are shown. **B,** mutational analysis of *NRAS*, *KRAS*, *MAP2K1*, *ARAF*, and *PIK3CA* from archival, formalin-fixed, paraffin embedded tissue from $BRAF^{V600E}$–wild-type patients with a spectrum of non-LCH neoplasms. Diagnosis and percent histiocyte content per section are shown in the first 2 rows. **C,** diagram of *MAP2K1* mutations identified by WES, RNA-seq, and targeted sequencing approaches in this study. **D,** diagram of activating *ARAF* mutations identified by WES, RNA-seq, and targeted sequencing approaches in the study. **E,** Western blot analysis of pERK1/2, pMEK1/2, and controls in 293T cells transfected with vector, wild-type (WT) FLAG-MEK1, or various FLAG-MEK1–mutant cDNAs along with HA-tagged ERK2.

expression by reverse transcription polymerase chain reaction (RT-PCR) with breakpoint-flanking primers, as well as with interphase FISH (Fig. 2A and B). Sequencing of the *RNF11–BRAF* fusion revealed that this transcript developed from an in-frame fusion of exon 1 of *RNF11* to exons 11 to 18 of *BRAF*. This results in loss of the N-terminal regulatory, RAS-binding domain in BRAF and placement of the BRAF kinase domain under the aberrant regulation of the *RNF11* promoter. Although *RNF11* is a novel *BRAF* fusion partner, the *RNF11–BRAF* fusion has a similar configuration to previously described *BRAF* fusions (17). Stable expression of RNF11–BRAF in cytokine-dependent, murine pro-B cell Ba/F3 cells, along with an empty vector, wild-type BRAF, or $BRAF^{V600E}$, revealed activation of ERK and MEK phosphorylation by both

Figure 2. Kinase fusions in non-LCH neoplasms. **A,** illustration of the *RNF11–BRAF* fusion with Sanger sequencing confirmation. **B,** *BRAF* FISH break-apart probes revealing an isolated green signal confirming translocation of *BRAF*. **C,** effect of stable expression of *BRAF* wild-type (WT), $BRAF^{V600E}$, *RNF11–BRAF*, or an empty vector on MAP kinase and AKT signaling, and (**D**) cytokine-independent growth of Ba/F3 cells. Mean viable cell number after IL3 withdrawal from a triplicate experiment is shown. Error bars, SD of mean. **E,** CellTiter-Glo luminescent viability IC_{50} results from three independent experiments of Ba/F3 cells from **D** exposed to MEK inhibitor GDC-0973, vemurafenib, or sorafenib. Log_{10} IC_{50} values are shown on the *y*-axis. Error bars, SEM. **F,** illustration of the *CLIP2–BRAF* fusion with Sanger sequencing confirmation identified in histiocytic ovarian infiltrates in a patient with non-LCH. **G,** illustration of the *KIF5B–ALK* fusion with Sanger sequencing confirmation. **H,** ALK FISH break-apart probe reveals an isolated red signal confirming the translocation of *ALK*. **I,** effect of *KIF5B–ALK* expression on ALK, STAT3, MEK1/2, ERK1/2, and AKT signaling in serum-starved Ba/F3 cells. **J,** effect of expression of *KIF5B–ALK* on cytokine-independent growth in Ba/F3 cells. Mean viable cell number after IL3 withdrawal from triplicate experiment is shown. Error bars, SD of the mean. **K,** CellTiter-Glo luminescent viability IC_{50} results from three independent experiments of Ba/F3 cells from **J** exposed to crizotinib or alectinib. Log_{10} IC_{50} values are shown on the y-axis. Error bars, SEM. **L,** illustration of a second *KIF5B–ALK* fusion identified in the liver lesions of a 50-year-old patient with ECD involving exons 1 to 24 of *KIF5B* and 20 to 29 of *ALK*. **M,** IHC of NTRK1 (top left) and CD68 (top right) in skin lesions of the *LMNA–NTRK1* fusion index patient (400× magnification; scale bar, 50 μm) and illustration of the *LMNA–NTRK1* fusion (bottom).

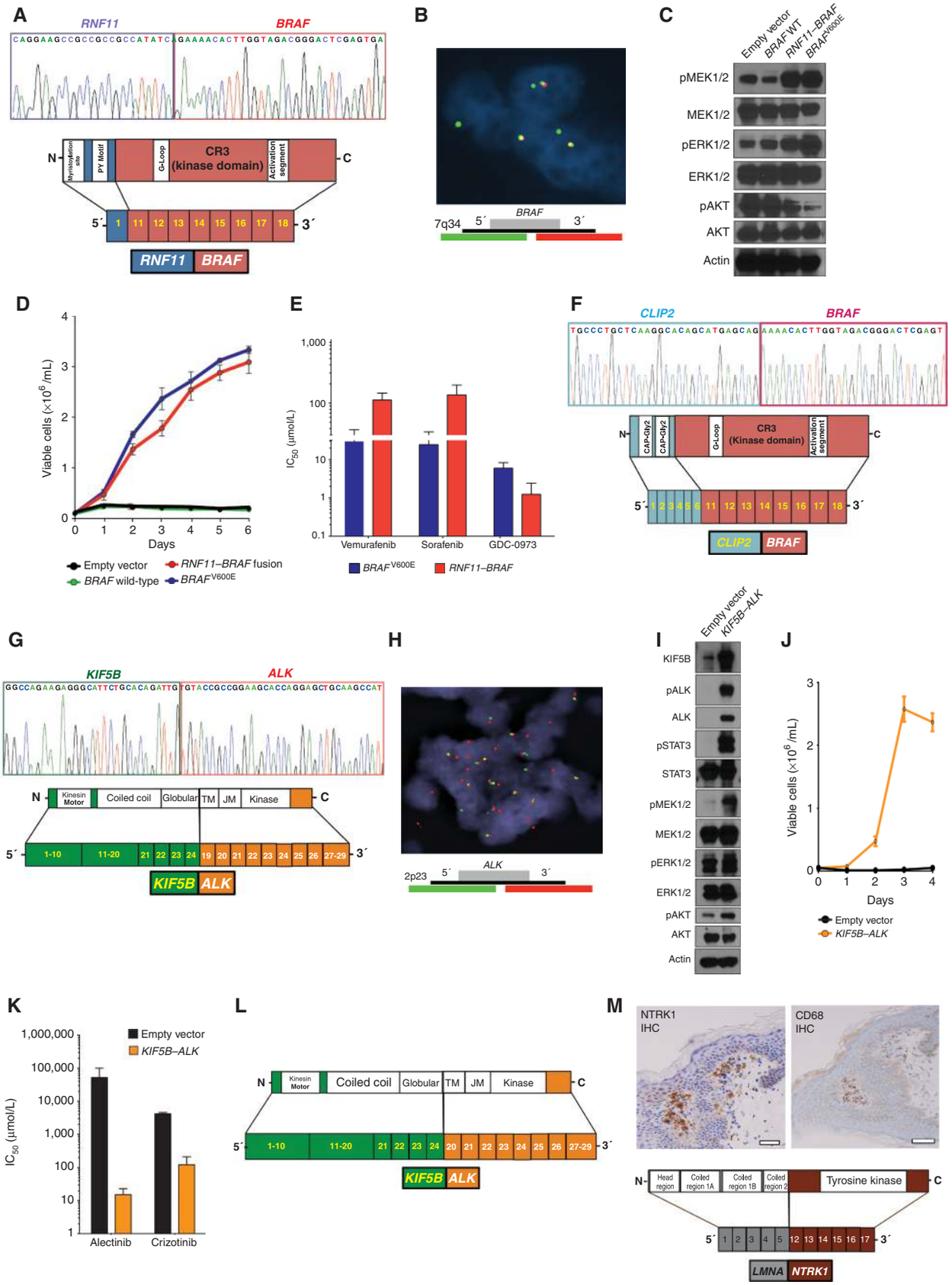

RNF11–BRAF and BRAF^{V600E} proteins (Fig. 2C). Likewise, expression of RNF11–BRAF or BRAF^{V600E} resulted in cytokine-independent growth of Ba/F3 cells (Fig. 2D), indicating that the *RNF11–BRAF* fusion is an activating event with pathway activity similar to the *BRAF*^{V600E} mutation. Moreover, RNF11–BRAF expression sensitized Ba/F3 cells to MEK inhibition but not to RAF inhibition by vemurafenib, similar to previous reports analyzing other *BRAF* fusion genes (18, 19; Fig. 2E).

Targeted RNA-seq analysis (20) of 9 patients with *BRAF*^{V600E}–wild-type, non-LCH using a panel of 265 genes known to be translocated in cancer detected an additional *BRAF* fusion. This was a *CLIP2–BRAF* fusion identified in retroperitoneal lesions from a patient with non-LCH, resulting in juxtaposition of the kinase domain of BRAF (exons 11–18) to the N-terminal domain of the protease CLIP2 (Fig. 2F). Expression was confirmed by RT-PCR/Sanger sequencing. As with the *RNF11–BRAF* fusion, this is a previously unreported fusion of *BRAF*.

In addition to *BRAF* fusions, an in-frame fusion of *KIF5B* (exons 1–24) to the kinase domain of *ALK* (exons 19–29) was identified in skin lesions from a 25-year-old with *BRAF*^{V600E}–wild-type ECD (Fig. 2G; Supplementary Fig. S4B). Expression was confirmed by RT-PCR/Sanger sequencing, interphase FISH, and IHC (Fig. 2G and H; Supplementary Fig. S4C). Although *KIF5B–ALK* fusions have been described in non–small cell lung cancer (NSCLC; ref. 21), this particular case harbored a unique breakpoint. In both tumor types, the kinase domain of ALK is fused to the N-terminal coiled-coil domain of KIF5B, resulting in inappropriate ALK expression, as well as constitutive ALK activation. Introduction of this patient's ALK fusion into Ba/F3 cells resulted in clear ALK, MAP kinase, STAT3, and PI3K–AKT pathway activation (Fig. 2I), as well as cytokine-independent growth (Fig. 2J). KIF5B–ALK-expressing cells, but not empty vector controls, were exquisitely sensitive to ALK inhibition (Fig. 2K). Interestingly, targeted RNA-seq analysis identified a second *KIF5B–ALK* fusion in the liver lesions of a 50-year-old patient with ECD (Fig. 2L). Finally, an *LMNA–NTRK1* fusion was identified in the skin lesions of a 27-year-old patient with ECD (Fig. 2M; Supplementary Fig. S4D). *LMNA–NTRK1* fusions have been identified in Spitzoid neoplasms (22) and result in aberrant NTRK1 expression with consequent MAP kinase and PI3K–AKT pathway activation.

Gene Expression Analysis of Langerhans and Non-Langerhans Histiocytic Neoplasms

Given the presence of *BRAF*^{V600E}, *MAP2K1*, and *ARAF* mutations in both LCH and non-LCH, we next performed gene expression analysis to understand potential biologic differences in these clinically distinct disorders. Unsupervised hierarchical clustering of the top 1% of differentially expressed genes (Supplementary Table S4; Fig. 3A) revealed that samples clustered first by clinical diagnosis (LCH or ECD) then by kinase alteration. Genes differentially expressed between LCH and ECD included all the genes known to encode proteins used to discriminate LCH from ECD histologically (ref. 1; Fig. 3B). Moreover, restriction of gene expression analyses to those LCH and non-LCH samples harboring *BRAF* mutations revealed the presence of a core set of genes discrepant between LCH and ECD (Fig. 3C and D; Supplementary Fig. S5A and S5B). First, this included strong enrichment of genes expressed in LCH samples from this study with prior gene expression data from purified CD207^{+} LCH tumor cells (23). In addition, LCH samples harbored strong enrichment of gene sets upregulated in late-stage myeloid progenitor cells and granulocyte–monocyte progenitors (GMP), as well as multiple gene sets from classic dendritic cells (cDC; Fig. 3C and Supplementary Fig. S5). In contrast, non-LCH demonstrated enrichment of multiple gene sets upregulated in hematopoietic stem cells (HSC), common myeloid progenitors (CMP), and monocytes. These differences in gene set enrichments were largely due to upregulation in LCH samples of genes known to be highly expressed in cDCs (including *IRF7*, *RUNX3*, *GPR82*, and *CCR7*; Fig. 3D; ref. 24). In contrast, genes known to be upregulated in HSCs, such as *BAALC* (25) and *ID1* (26), as well as core macrophage-associated genes, such as *CEBPA* (27), were upregulated in non-LCH samples compared with LCH (Fig. 3D). In addition to gene sets related to hematopoietic ontogeny, gene sets involved in cell-cycle regulation and IL1 signaling were found to be enriched in LCH but not in ECD. Conversely, genes involved in lipid metabolism and adipogenesis were uniquely enriched in ECD but not in LCH (Supplementary Fig. S5). Although this result is consistent with the histologic appearance of ECD lesions, these data highlight a potential role of adipogenesis not previously recognized in this disorder.

Therapeutic Targeting of *MAP2K1*– and *ARAF*-Mutant Refractory Histiocytoses

Three of the investigated non-LCH patients with refractory disease and progressive organ dysfunction were treated with targeted therapies based on the discovery of novel kinase alterations described above. A *MAP2K1*^{K57N} mutation was noted from WES of perirenal lesions from a 53-year-old patient with ECD with progressive disease following treatment with both IFNα and anakinra, who was symptomatic by way of inflammatory ascites and renal failure. Treatment was initiated with a MEK inhibitor (single-agent trametinib 2 mg daily), resulting in abrupt cessation of ascitic accumulation and normalization of creatinine. Additionally, there was metabolic resolution of FDG-avid infiltrates in the retroperitoneum (SUV 8.2) and spermatic cords (SUV 6.2) to background SUV (Fig. 4A and B). The patient has been maintained on trametinib single-agent therapy with a sustained clinical response for >180 days. Similarly, treatment of a second patient with ECD with *MAP2K1*^{Q56P}-mutant disease refractory to 4 lines of prior therapy led to resolution of PET-avid disease in renal (SUV 8.4), aortic (SUV 3.9), and maxillary sinus (SUV 9.5) infiltrations to background SUV within a single month of administration of the MEK inhibitor cobimetinib (Fig. 4C).

Further evidence of effective targeted inhibition was found in a patient with ECD with disease in the bones, orbits, cavernous sinuses, and choroid, whose tumor was found to harbor an *ARAF*^{S214A} mutation. This patient's disease had progressed following cladribine, clofarabine, and anakinra. The patient was also symptomatic with visual impairment from macular edema that required ongoing corticosteroids (Fig. 4D; Supplementary Fig. S3A and S3B). Given a recent report of complete response to sorafenib in a patient with NSCLC with an *ARAF*^{S214C} mutation (28), we initiated

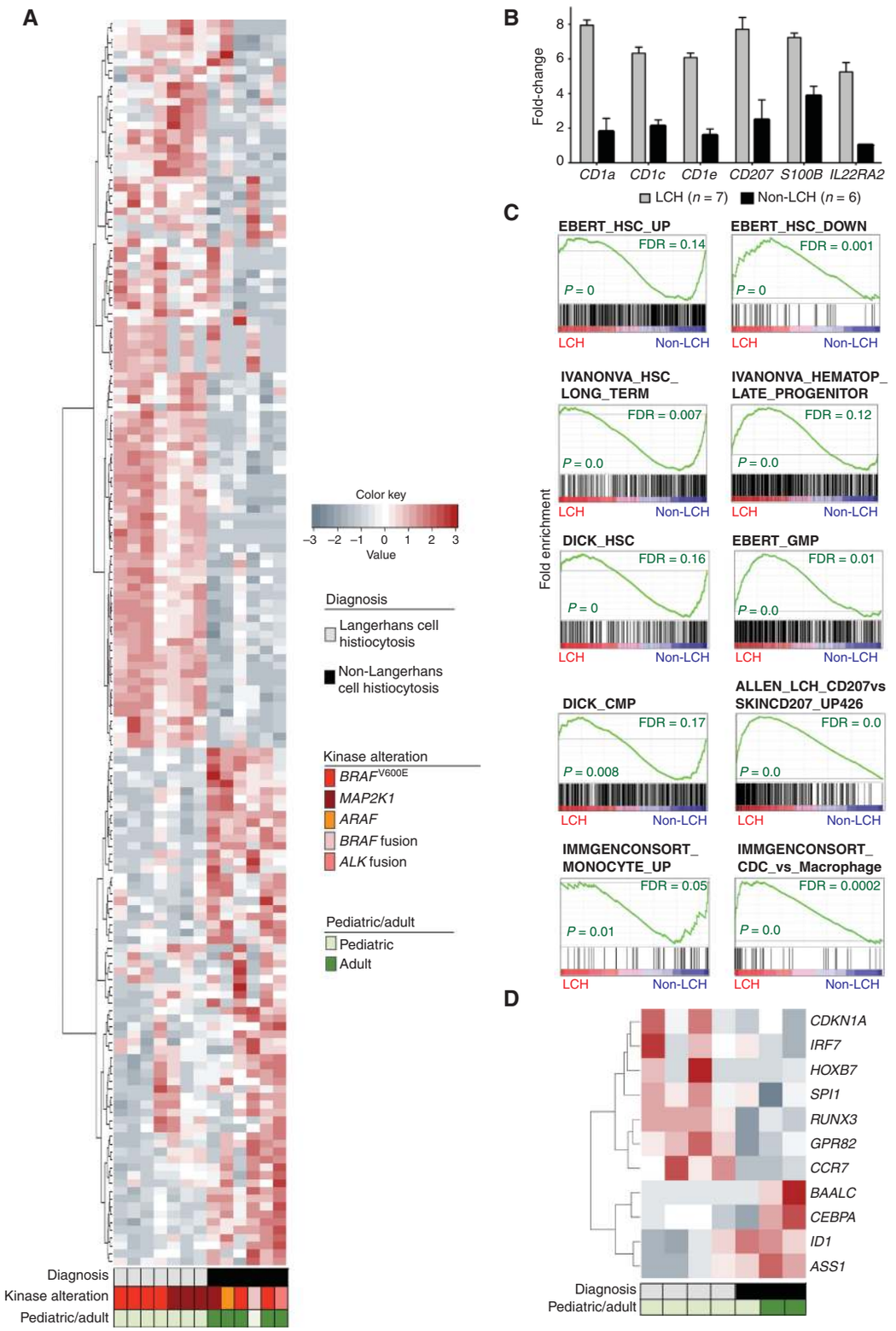

Figure 3. Gene expression analysis of histiocytic neoplasms by RNA-seq. **A,** unsupervised hierarchical clustering of the top 1% most differentially expressed genes in 7 LCH and 6 non-LCH lesions presented in a heat map. **B,** gene expression by RNA-seq of 6 of the 159 genes from **A**, which encode proteins currently known to differentiate these diseases in clinical diagnosis. **C,** enrichment plots of gene sets differentially enriched in LCH ($n = 4$) or non-LCH ($n = 3$) as detected by gene set enrichment analysis (analysis restricted to those samples with *BRAF* alterations only). **D,** eleven lineage-defining genes with enriched expression in LCH (4 cases) or non-LCH samples (3 cases) with *BRAF* kinase alterations.

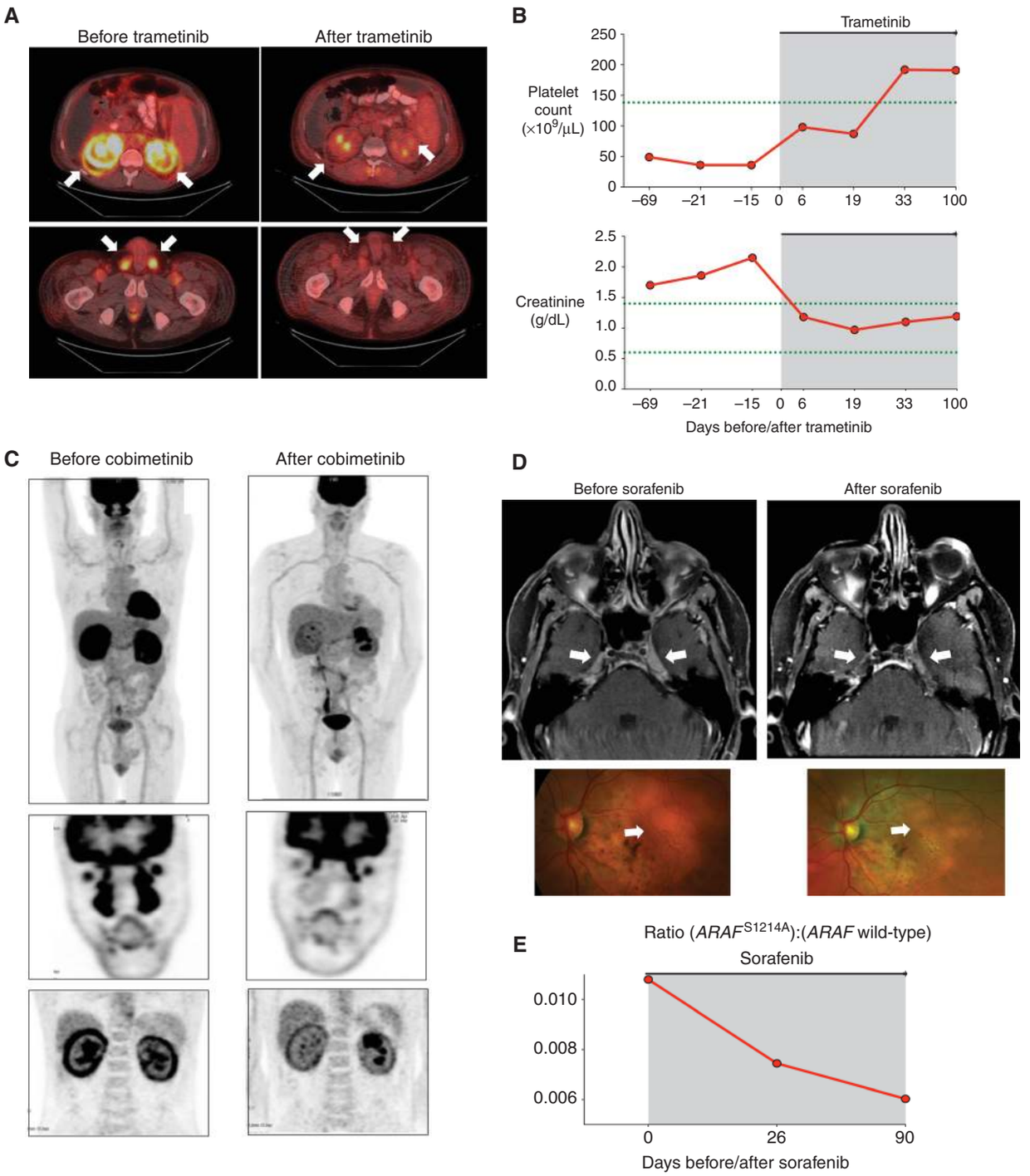

Figure 4. Therapeutic efficacy of MEK and RAF inhibition in patients with *MAP2K1*- and *ARAF*-mutant systemic histiocytic neoplasms. **A,** axial FDG-PET scans before trametinib and 4 weeks after trametinib in a patient with *MAP2K1*^{K57N} ECD with histiocytic infiltration of kidneys (top) and spermatic cord (bottom). **B,** creatinine and platelet counts in same patient before and after trametinib therapy (green line, boundary of normal values). **C,** PET scan before cobimetinib and 4 weeks after cobimetinib of a patient with *MAP2K1*^{Q56P}-mutant ECD with disease infiltration in facial sinuses, heart, and kidneys. **D,** axial brain MRI of a patient with *ARAF*^{S214A}-mutant ECD with histiocytic infiltration of retina and optic nerves. MRI images show optic nerve infiltration (arrows) before and 6 weeks after sorafenib (top). Retinal fundoscopic photographs from the same time points (bottom) reveal improvement in retinal infiltrates with sorafenib treatment. **E,** ratio of concentration of *ARAF*^{S214A}:*ARAF* wild-type in plasma cell–free DNA with sorafenib treatment.

sorafenib therapy, titrated up to 600 mg daily. Within 12 weeks, there was regression of lesions in the cavernous sinuses (by post-gadolinium MRI) and retina (as visualized directly by fundoscopy), and the patient was able to taper her steroid dose. This coincided with a >50% decrease in mutant *ARAF* DNA in plasma cell–free DNA (Fig. 4E).

DISCUSSION

Systemic histiocytic neoplasms constitute a broad spectrum of disorders that are characterized by the accumulation of abnormal, mononuclear, phagocyte-derived cells within infiltrative granulomatous lesions in nearly any organ (1). The rarity of histiocytic disorders combined with their protean clinical manifestations has resulted in great uncertainty about their pathogenesis for decades. The discovery of *BRAF*^{V600E} mutations in LCH (2, 3) and ECD (4), followed by the identification of *MAP2K1* mutations in LCH (10–12), however, resulted in a new understanding of histiocytic neoplasms as myeloid-derived disorders driven by activating mutations affecting the MAP kinase pathway (3). In fact, nearly all cases of LCH and ECD have been demonstrated to have the prominent presence of activated ERK within lesional tissue (2). This has led to the hypothesis that histiocytic neoplasms contain mutations affecting the MAP kinase pathway in 100% of patients. Despite this, the cellular heterogeneity of histiocytic lesions combined with their frequent occurrence in sites unamenable to biopsy (such as brain and heart) has presented challenges to identifying the full constellation of genomic alterations in an unbiased manner. As a result, technologies such as RNA-seq, for example, have never been performed in histiocytic neoplasms, and mutations that coexist with MAP kinase alterations are undefined in these disorders.

Through the efforts of an international collaboration to unravel the molecular bases of these disorders in an unbiased manner, we combined WES and RNA-seq of fresh-frozen biopsies from patients with histiocytic disorder and identified a spectrum of activating kinase alterations in 100% of cases. This includes the first description of kinase fusions in systemic histiocytic neoplasms and *ARAF* and *MAP2K1* mutations in non-LCH. The identification of fusions involving *BRAF*, *ALK*, and *NTRK1* in patients with non-LCH further enriches the number of genomic alterations shared between histiocytic neoplasms and common malignancies such as NSCLC. Moreover, kinase fusions may provide further novel therapeutic targets for patients with histiocytosis. For example, patients with histiocytosis bearing *ALK* fusions may be amenable to ALK inhibitors, as these have demonstrated efficacy in *ALK*-rearranged NSCLC (29, 30). In addition, those patients expressing *NTRK* fusions might be eligible for ongoing clinical trials utilizing novel TRK inhibitors (31).

Although mutations in genes involved in diverse biologic processes and pathways co-occurring with activating kinase alterations were identified here, future efforts with larger sequencing cohorts will be needed to determine if there are differences in mutational patterns between LCH and non-LCH. In addition, due to the heterogeneity of cells in systemic histiocytoses lesions, the overall VAFs of somatic mutations identified here were low, precluding our ability to determine the clonal composition of these tumors. Furthermore, although coexisting activating kinase alterations involving *BRAF*^{V600E} and *ARAF* or compound *ARAF* mutations have been described in LCH (10, 32) and now in non-LCH based on our study, very little is currently known about the mechanistic consequences of *ARAF* mutations on MAP kinase signaling. Thus, future efforts will be needed to understand the basis for this scenario of *ARAF* mutations coexisting with additional MAP kinase pathway mutations.

Overall, mutations in *MAP2K1* and *ARAF* were the most common kinase alterations among *BRAF*^{V600E}–wild-type patients. The clinical responses of *MAP2K1*- and *ARAF*-mutant ECD to therapies targeted against these alterations may overhaul the landscape of treatment for severe forms of *BRAF*^{V600E}–wild-type non-LCH, mandating prospective clinical trials of these agents, as have been performed for *BRAF*^{V600E}-mutant histiocytoses (33). The rapid and sustained clinical responses to MEK inhibition in this study are particularly significant in light of the fact that single-agent MEK inhibition has not demonstrated robust clinical benefit in the context of other *BRAF/RAS*-mutant malignancies previously (34–36). It is possible that the relatively small number of mutations per exome in histiocytic neoplasms seen here compared with those in common malignancies, such as melanoma (37) and NSCLC (38, 39), may account for the remarkable and sustained clinical responses of histiocytoses to single-agent RAF or MEK inhibition.

In addition to the identification of kinase fusions, RNA-seq analyses also identified important transcriptional profiles in LCH and non-LCH, which appear to be distinct from one another. These data suggest the intriguing possibility that LCH has a gene expression profile most similar to cDCs and late-stage myeloid progenitor cells and reinforce prior reports that suggest LCH is derived from immature myeloid dendritic cells (3). In contrast, non-LCH lesions appear to share transcriptional profiles more similar to monocytes and earlier hematopoietic stem and progenitor cells. These data represent the first attempt to identify the cell-of-origin of non-LCH using transcriptomic data, which will be important to validate in future efforts, and further refine our knowledge of the cell-of-origin of LCH.

Overall, these findings demonstrate the need for comprehensive genomic analysis of these rare and diverse tumor types, as they may directly affect clinical therapy for patients with histiocytosis. Further efforts to integrate genomic analysis into the clinical care of patients with histiocytic disorder may greatly help in both disease classification and therapeutic decision making for these patients.

METHODS

Patients

The study was conducted according to the Declaration of Helsinki, and human tissues were obtained with patient-informed consent under approval by the Institutional Review Boards of Memorial Sloan Kettering Cancer Center, St. Jude Children's Research Hospital, The University of Texas MD Anderson Cancer Center, the National Human Genome Research Institute, and Pitié-Salpêtrière Hospital.

Excised lesions were either flash-frozen for DNA/RNA extraction and/or fixed in 4% neutral-buffered formalin, embedded in paraffin, and processed by routine histologic methods. For patients undergoing WES, DNA extracted from peripheral blood mononuclear cells

was utilized as a paired germline control. In total, specimens from 64 patients were analyzed, and the clinical, histologic, and genetic characteristics are summarized in Supplementary Tables S1 and S3.

Whole-Exome Sequencing

Analysis of exome sequencing data, which includes mapping, coverage and quality assessment, single-nucleotide variant (SNV)/indel detection, tier annotation for sequence mutations, and prediction of deleterious effects of missense mutations, has been described previously (40, 41). Approximately 250 ng of DNA from each sample was sheared to an average of 150 bp in a Covaris instrument for 360 seconds (duty cycle, 10%; intensity, 5; cycles/burst, 200). Bar-coded libraries were prepared using the Kapa Low-Throughput Library Preparation Kit Standard (Kapa Biosystems), amplified using the KAPA HiFi Library Amplification Kit (Kapa Biosystems; 8 cycles), and quantified using Qubit Fluorimetric Quantitation (Invitrogen) and Agilent Bioanalyzer. An equimolar pool of the 4 bar-coded libraries (300 ng each) was used as input to capture the exome using one reaction tube of the Nimblegen SeqCap EZ Human Exome Library v3.0 (Roche; cat no. 06465684001), according to the manufacturer's protocol. The pooled capture library was quantified by Qubit (Invitrogen) and Bioanalyzer (Agilent) and sequenced on an Illumina HiSeq 2500 using a paired end, 100 nucleotide in length run mode, to achieve an average of 100× coverage.

Confirmation of Mutations

The following mutations in genes coding tyrosine kinases were confirmed using ddPCR: *ARAF* S214A, S186R, A225V, and P539H; *BRAF* V600E and R603Q; *MAP2K1* K57N, F53_Q58del, Q58_E62del, and F68L; *NRAS* Q61R, and *PIK3CA* E542K, using BioRad probes with FAM for the mutants and HEX for the wild-type sequences, on a BioRad QX200 ddPCR system, following the manufacturer's instructions, starting from 30 ng of template DNA. For the rest of the mutations, we used a custom-designed, TruSeq Custom Amplicon probe to confirm the mutations detected by exome sequencing. Design Studio (Illumina) was used to design amplicons covering the regions of interest. The regions were amplified using 250 ng of template genomic DNA, using the manufacturer's instructions, with 25 cycles of amplification, and were run on an Illumina MiSeq 2 × 250 cartridge.

RNA Sequencing

RNA library construction for transcriptome sequencing was done as per the manufacturer's instructions using the Illumina TruSeq RNA sample preparation V2. Sequencing was completed on the Illumina HiSeq 2000 as per the manufacturer's instructions. Analysis of transcriptome sequencing data, which includes mapping, coverage, and quality assessment, SNV/indel detection, tier annotation for sequence mutations, and prediction of deleterious effects of missense mutations, has been described previously (40, 41). For gene expression analyses, transcript expression levels were estimated as fragments per kilobase of transcript per million mapped reads (FPKM); gene FPKMs were computed by summing the transcript FPKMs for each gene using Cuffdiff2 (42, 43). A gene was considered "expressed" if the FPKM value was ≥0.5 based on the distribution of FPKM gene expression levels. Genes that were not expressed in any sample group were excluded from the final data matrix for downstream analysis. Gene set enrichment analysis (GSEA) was performed as described previously (44), and the methodology and approach are described in the Supplementary Methods.

Targeted DNA Sequencing

We sequenced the regions of known mutations in *MAP2K1*, *NRAS*, *KRAS*, and *PIK3CA*, as well as all coding exons of *ARAF*, using Sanger sequencing (primer sequences listed in Supplementary Table S5) and/or hybrid-capture, next-generation sequencing using the MSKCC IMPACT assay as previously described (45) or the Foundation One Assay (Foundation Medicine, Inc.), as previously described (46). Prior to DNA extraction, FFPE samples from all cases were reviewed to confirm that the tissue was of sufficient size to generate a minimum of 50 ng of 20% histiocyte nucleic acid. DNA was isolated from 40-μm-thick sections of FFPE tissue.

Targeted RNA Sequencing

Total RNA extracted from 40-μm-thick sections of FFPE tumor was reverse transcribed with random hexamer primers using the Super-Script III First-Strand Synthesis System (Invitrogen). Double-stranded cDNA was synthesized with the NEBNext mRNA Second Strand Synthesis Module (New England BioLabs). Hybrid selection of indexed, adaptor-ligated libraries was performed using the cDNA Kinome hybridization kit with 612 transcripts of kinases and kinase-related genes (Agilent SureSelect Human Kinome Kit). Selected libraries were sequenced on the HiSeq-2000 instrument (Illumina) with 49 × 49 paired reads. For RNA sequencing, we used a sequencing approach targeting 612 transcripts of kinases and kinase-related genes. We aimed for a high number of unique read pairs (~50,000,000) per sample (Supplementary Table S2).

Gene Fusion Confirmation

All gene fusions were validated with RT-PCR followed by direct sequencing, interphase FISH, and/or immunohistochemical analysis. RT-PCR was performed from cDNA (primer sequences available upon request), followed by analysis on a Bioanalyzer (Agilent). Specific PCR amplicons were detected only with the appropriate combination of primer and template and not with negative controls. The nucleotide sequence at the fusion site was confirmed with Sanger sequencing. Details of interphase FISH are included in the Supplementary Methods.

Plasma Cell–Free DNA (cfDNA) Collection and Analysis by ddPCR

Blood (10 mL) was collected into Streck tubes, and plasma was then separated from blood using standard techniques. Plasma cfDNA was isolated using the QIAamp Circulating Nucleic Acid Kit (Qiagen) according to the manufacturer's instructions, and the concentration was assessed using a BioAnalyzer.

The S214A (c.640T>G) mutation for *ARAF* was evaluated by ddPCR (BioRad QX200) in a custom-designed, allele-specific assay (primer sequences available upon request). The experiments were performed using the following protocol: 1 cycle at 95°C for 10 minutes, 40 cycles at 94°C for 30 seconds and 55°C for 1 minute, 1 cycle at 98°C for 10 minutes, then held at 4°C, all at a ramp rate of 2°C/second. BioRad's T100 thermal cycler was used for the PCR step. When available, 5 ng of DNA was assessed in a 20 μL PCR reaction, partitioned into approximately 20,000 droplets. A total of two replicates were used per sample. Droplets were quantified using the BioRad Quantasoft Software (version 7.0) to identify the concentration of $ARAF^{S214A}$-mutant copies/mL DNA and of *ARAF* wild-type copies/mL of DNA. The ratio of the concentration of mutant to wild-type *ARAF* ([Mu]/[WT]) was then calculated for each patient pretreatment and following 1 and 3 months of sorafenib therapy.

Germline DNA Mutational Analysis

An automated analysis of mutations from the WES of germline DNA was performed to search for pathologic mutations in 565 cancer associated genes, including 60 autosomal dominant cancer predisposition genes (*ALK*, *APC*, *BAP1*, *BMPR1A*, *BRAF*, *BRCA1*, *BRCA2*, *CBL*, *CDC73*, *CDH1*, *CDK4*, *CDKN1C*, *CDKN2A*, *CEBPA*,

DICER1, *EPCAM*, *FH*, *GATA2*, *HRAS*, *KRAS*, *MAP2K1*, *MAP2K2*, *MAX*, *MEN1*, *MLH*, *MSH2*, *MSH6*, *NF1*, *NF2*, *NRAS*, *PALB2*, *PAX5*, *PHOX2B*, *PMS2*, *PRKAR1A*, *PTCH1*, *PTEN*, *PTPN11*, *RAF1*, *RB1*, *RET*, *RUNX1*, *SDHA*, *SDHAF2*, *SDHB*, *SDHC*, *SDHD*, *SHOC2*, *SMAD4*, *SMARCA4*, *SMARCB1*, *SOS1*, *STK11*, *SUFU*, *TMEM127*, *TP53*, *TSC1*, *TSC2*, *VHL*, and *WT1*), as well as all genes previously reported to be mutated in individuals with clonal hematopoiesis associated with a somatic mutation (*ASXL1*, *DNMT3A*, *FLT3*, *GNAS*, *GNB1*, *IDH1*, *IDH2*, *JAK2*, *KIT*, *NPM1*, *SF3B1*, *SRSF2*, *TET2*, *U2AF1*, and others; refs. 13–15, 47). With the exception of variants that matched those contained within the IARC *TP53* database, only novel, nonsilent SNVs or SNVs with <0.1% population frequency in the NHLBI ESP database received an automatic classification. In-frame indels that matched the Single Nucleotide Polymorphism Database (dbSNP) did not receive a classification. Indels present in 1000 Genomes or with multiple submissions in dbSNP were also excluded.

To identify pathologic lesions, variants were classified into three tiers, named gold, silver, and bronze. Gold was reserved for truncation mutations in tumor suppressor genes, matches to truncation mutations and hotspot mutations in somatic mutation database, and perfect matches to highly curated locus-specific databases, including the IARC *TP53* database, NHGRI *BRCA1* and *BRCA2* database for records marked clinically important, ARUP *MEN2* database for mutations in *RET*, ASU database for *TERT* mutations, the Leiden Open Variation Database (LOVD) for mutations in *APC* and *MSH2*, and the *RB1* mutation database. Silver was used for variants of less certain significance, and bronze for variants more likely to be benign. Additional databases that were utilized for classification included HGMD, ClinVar, and UMD, matches to which generally received a silver classification. Truncation mutations located close to the C-terminus of the protein that did not map to a functional domain were examined manually, and we consulted with external gene experts for their pathogenicity.

Drug Studies

Vemurafenib, sorafenib, GDC-0973 (cobimetinib), crizotinib, and alectinib were purchased from Selleckchem. Drug studies were conducted *in vitro* using FACS-sorted, $DAPI^-$ $eGFP^+$ Ba/F3 cells that stably expressed the MIGII-EV, MIGII-*BRAF*^{V600E}, MIGII-*RNF11–BRAF*, and MIGII-*KIF5B–ALK* constructs using the CellTiter-Glo Luminescent Cell Viability Assay from Promega Corporation, according to the manufacturer's instructions. The MIGII-*BRAF*^{V600E}, MIGII-*RNF11–BRAF*, and MIGII-*KIF5B–ALK* FACS-sorted Ba/F3 cells were maintained in RPMI + 10% FBS + penicillin and streptomycin media without murine IL3, and MIGII-EV was maintained in RPMI + 10% FBS + penicillin and streptomycin with recombinant murine IL3 (1 ng/mL).

GSEA

GSEA was performed as described previously (3). The dataset was converted to gene symbols, and the gene expression signatures were analyzed using the java GSEA package. The most differentially expressed genes for each comparison were used to generate a signature for GSEA analysis. The input motif gene sets were extracted from the Molecular Signature Database, version 4 (MSigDBv4). Gene sets with a $P < 0.05$ and a false discovery rate (FDR) q-value < 25% were considered to be significantly enriched in LCH and non-LCH cases evaluated by RNA-seq.

Accession Codes

Whole-exome ($n = 24$ patients) and transcriptome ($n = 13$) sequencing data for the patients from the discovery cohort have been deposited in the Sequence Read Archive (SRA) and Gene Expression Omnibus (GEO), respectively. The SRA accession number is SRP065600, and the GEO accession number is GSE74442.

Disclosure of Potential Conflicts of Interest

J. Estrada-Veras is a consultant/advisory board member for the Erdheim–Chester Disease Global Alliance. M. Lacouture reports receiving commercial research grants from and is a consultant/advisory board member for Genentech and Roche. P.J. Stephens has ownership interest in Foundation Medicine. V.A. Miller has ownership interest in Foundation Medicine. J.S. Ross reports receiving a commercial research grant from and has ownership interest in Foundation Medicine. D.B. Solit is a consultant/advisory board member for Pfizer. D.M. Hyman is a consultant/advisory board member for Atara Biotherapeutics and Chugai. F. Janku reports receiving commercial research grants from Biocartis, Foundation Medicine, and Trovagene and is a consultant/advisory board member for Trovagene. A. Dogan is a consultant/advisory board member for Cancer Genetics. J.-F. Emile is a consultant/advisory board member for Roche and GlaxoSmithKline. N. Rosen reports receiving a commercial research grant from Chugai and is a consultant/advisory board member for AstraZeneca, Chugai, Kura, and Millennium-Takeda. No potential conflicts of interest were disclosed by the other authors.

One of the Editors-in-Chief is an author on this article. In keeping with the AACR's editorial policy, the peer review of this submission was managed by a senior member *of Cancer Discovery*'s editorial team; a member of the AACR Publications Committee rendered the final decision concerning acceptability.

Authors' Contributions

Conception and design: E.L. Diamond, B.H. Durham, J. Haroche, S.A. Parikh, F. Cohen-Aubart, M. Lacouture, J.S. Ross, D.B. Solit, D.M. Hyman, J. Baselga, Z. Amoura, J.-F. Emile, T.A. Gruber, O. Abdel-Wahab

Development of methodology: B.H. Durham, J. Haroche, J. Choi, I. Dolgalev, M. Lacouture, J.S. Ross, D.B. Solit

Acquisition of data (provided animals, acquired and managed patients, provided facilities, etc.): E.L. Diamond, B.H. Durham, Z. Yao, S.A. Parikh, J. Choi, E. Kim, F. Cohen-Aubart, S.C.-W. Lee, Y. Gao, J.-B. Micol, P. Campbell, B. Sylvester, O. Aminova, A. Heguy, P. Zappile, J. Nakitandwe, C. Ganzel, J.D. Dalton, D.W. Ellison, J. Estrada-Veras, M. Lacouture, V.A. Miller, J.S. Ross, S.M. Ali, S.R. Briggs, O. Fasan, J. Block, S. Héritier, J. Donadieu, D.B. Solit, D.M. Hyman, F. Janku, C.Y. Park, Z. Amoura, A. Dogan, J.-F. Emile, O. Abdel-Wahab

Analysis and interpretation of data (e.g., statistical analysis, biostatistics, computational analysis): E.L. Diamond, B.H. Durham, J. Haroche, Z. Yao, J. Ma, Z. Wang, F. Cohen-Aubart, S.C.-W. Lee, M.P. Walsh, I. Dolgalev, A. Heguy, C. Ganzel, J.D. Dalton, D.W. Ellison, M. Lacouture, P.J. Stephens, J.S. Ross, S.M. Ali, F. Janku, B.S. Taylor, Z. Amoura, A. Dogan, J.-F. Emile, N. Rosen, O. Abdel-Wahab

Writing, review, and/or revision of the manuscript: E.L. Diamond, B.H. Durham, J. Haroche, S.A. Parikh, Z. Wang, F. Cohen-Aubart, J.-B. Micol, P. Campbell, D.W. Ellison, J. Estrada-Veras, M. Lacouture, P.J. Stephens, V.A. Miller, J.S. Ross, S.M. Ali, J. Donadieu, D.B. Solit, D.M. Hyman, J. Baselga, F. Janku, A. Dogan, J.-F. Emile, N. Rosen, T.A. Gruber, O. Abdel-Wahab

Administrative, technical, or material support (i.e., reporting or organizing data, constructing databases): E.L. Diamond, B.H. Durham, E. Kim, I. Dolgalev, P. Zappile, M. Lacouture, J.S. Ross, S.M. Ali, S.R. Briggs, S. Héritier, D.M. Hyman, J.-F. Emile

Study supervision: E.L. Diamond, B.H. Durham, W.A. Gahl, J.S. Ross, J. Baselga, T.A. Gruber, O. Abdel-Wahab

Other (performed organic extraction of RNA, quality and quantification of RNA): J. Nakitandwe

Other (support for contributing investigator): W.A. Gahl

Acknowledgments

The authors thank Vincent Gazin (French Medical Agency) for help with acquisition of cobimetinib, Kristen O'Dwyer (University of

Rochester) for help with patient care, and Brian Marr for fundoscopic photographs.

Grant Support

B.H. Durham is supported by the American Society of Hematology Senior Research Training Awards for Fellows. E.L. Diamond, D.M. Hyman, and O. Abdel-Wahab are supported by grants from Erdheim–Chester Disease Global Alliance, the Society of Memorial Sloan Kettering Cancer Center (MSKCC), the Geoffrey Beene Research Center of MSKCC, and Translational and Integrative Medicine Research Fund of MSKCC. E. Kim is supported by the Worldwide Cancer Research Fund. O. Abdel-Wahab is supported by an NIH K08 Clinical Investigator Award (1K08CA160647-01), the Josie Robertson Investigator Program, and a Damon Runyon Clinical Investigator Award with support from the Evans Foundation.

Received July 28, 2015; revised November 10, 2015; accepted November 11, 2015; published OnlineFirst November 13, 2015.

REFERENCES

1. Jaffe R, Pileri SA, Facchetti F, Jones DM, Jaffe ES. Histiocytic and dendritic cell neoplasms, Introduction. In: Swerdlow SH, Campo E, Harris NL, Jaffe ES, Pileri SA, Stein H, Thiele J, Vardiman JW, editors. WHO classification of tumours of haematopoietic and lymphoid tissues, 4th ed. Lyon: WHO Press; 2008. p. 354–5.
2. Badalian-Very G, Vergilio J-A, Degar B, MacConaill L, Brandner B, Calicchio M, et al. Recurrent BRAF mutations in Langerhans cell histiocytosis. Blood 2010;116:1919–23.
3. Berres ML, Lim KP, Peters T, Price J, Takizawa H, Salmon H, et al. BRAF-V600E expression in precursor versus differentiated dendritic cells defines clinically distinct LCH risk groups. J Exp Med 2014;211:669–83.
4. Haroche J, Charlotte F, Arnaud L, von Deimling A, Helias-Rodzewicz Z, Hervier B, et al. High prevalence of $BRAF^{V600E}$ mutations in Erdheim–Chester disease but not in other non-Langerhans cell histiocytoses. Blood 2012;120:2700–3.
5. Haroche J, Cohen-Aubart F, Emile J-F, Arnaud L, Maksud P, Charlotte F, et al. Dramatic efficacy of vemurafenib in both multisystemic and refractory Erdheim–Chester disease and Langerhans cell histiocytosis harboring the $BRAF^{V600E}$ mutation. Blood 2013;121:1495–500.
6. Haroche J, Cohen-Aubart F, Emile JF, Maksud P, Drier A, Toledano D, et al. Reproducible and sustained efficacy of targeted therapy with vemurafenib in patients with BRAF(V600E)-mutated Erdheim–Chester disease. J Clin Oncol 2015;33:411–8.
7. Hyman DM, Diamond EL, Vibat CR, Hassaine L, Poole JC, Patel M, et al. Prospective blinded study of $BRAF^{V600E}$ mutation detection in cell-free DNA of patients with systemic histiocytic disorders. Cancer Discov 2015;5:64–71.
8. Heritier S, Jehanne M, Leverger G, Emile JF, Alvarez JC, Haroche J, et al. Vemurafenib use in an infant for high-risk Langerhans cell histiocytosis. JAMA Oncol 2015;1:836–8.
9. Diamond EL, Dagna L, Hyman DM, Cavalli G, Janku F, Estrada-Veras J, et al. Consensus guidelines for the diagnosis and clinical management of Erdheim–Chester disease. Blood 2014;124:483–92.
10. Chakraborty R, Hampton OA, Shen X, Simko SJ, Shih A, Abhyankar H, et al. Mutually exclusive recurrent somatic mutations in MAP2K1 and BRAF support a central role for ERK activation in LCH pathogenesis. Blood 2014;124:3007–15.
11. Brown NA, Furtado LV, Betz BL, Kiel MJ, Weigelin HC, Lim MS, et al. High prevalence of somatic MAP2K1 mutations in $BRAF^{V600E}$-negative Langerhans cell histiocytosis. Blood 2014;124:1655–8.
12. Nelson DS, van Halteren A, Quispel WT, van den Bos C, Bovee JV, Patel B, et al. MAP2K1 and MAP3K1 mutations in Langerhans cell histiocytosis. Genes Chromosomes Cancer 2015;54:361–8.
13. Jaiswal S, Fontanillas P, Flannick J, Manning A, Grauman PV, Mar BG, et al. Age-related clonal hematopoiesis associated with adverse outcomes. N Engl J Med 2014;371:2488–98.
14. Genovese G, Kahler AK, Handsaker RE, Lindberg J, Rose SA, Bakhoum SF, et al. Clonal hematopoiesis and blood-cancer risk inferred from blood DNA sequence. N Engl J Med 2014;371:2477–87.
15. Xie M, Lu C, Wang J, McLellan MD, Johnson KJ, Wendl MC, et al. Age-related mutations associated with clonal hematopoietic expansion and malignancies. Nat Med 2014;20:1472–8.
16. Emile JF, Diamond EL, Helias-Rodzewicz Z, Cohen-Aubart F, Charlotte F, Hyman DM, et al. Recurrent RAS and PIK3CA mutations in Erdheim–Chester disease. Blood 2014;124:3016–9.
17. Palanisamy N, Ateeq B, Kalyana-Sundaram S, Pflueger D, Ramnarayanan K, Shankar S, et al. Rearrangements of the RAF kinase pathway in prostate cancer, gastric cancer and melanoma. Nat Med 2010;16:793–8.
18. Hutchinson KE, Lipson D, Stephens PJ, Otto G, Lehmann BD, Lyle PL, et al. BRAF fusions define a distinct molecular subset of melanomas with potential sensitivity to MEK inhibition. Clin Cancer Res 2013;19:6696–702.
19. Sievert AJ, Lang SS, Boucher KL, Madsen PJ, Slaunwhite E, Choudhari N, et al. Paradoxical activation and RAF inhibitor resistance of BRAF protein kinase fusions characterizing pediatric astrocytomas. Proc Natl Acad Sci U S A 2013;110:5957–62.
20. Chmielecki J, Hutchinson KE, Frampton GM, Chalmers ZR, Johnson A, Shi C, et al. Comprehensive genomic profiling of pancreatic acinar cell carcinomas identifies recurrent RAF fusions and frequent inactivation of DNA repair genes. Cancer Discov 2014;4:1398–405.
21. Takeuchi K, Choi YL, Togashi Y, Soda M, Hatano S, Inamura K, et al. KIF5B–ALK, a novel fusion oncokinase identified by an immunohistochemistry-based diagnostic system for ALK-positive lung cancer. Clin Cancer Res 2009;15:3143–9.
22. Wiesner T, He J, Yelensky R, Esteve-Puig R, Botton T, Yeh I, et al. Kinase fusions are frequent in Spitz tumours and spitzoid melanomas. Nat Commun 2014;5:3116.
23. Allen CE, Li L, Peters TL, Leung HC, Yu A, Man TK, et al. Cell-specific gene expression in Langerhans cell histiocytosis lesions reveals a distinct profile compared with epidermal Langerhans cells. J Immunol 2010;184:4557–67.
24. Miller JC, Brown BD, Shay T, Gautier EL, Jojic V, Cohain A, et al. Deciphering the transcriptional network of the dendritic cell lineage. Nat Immunol 2012;13:888–99.
25. Baldus CD, Tanner SM, Kusewitt DF, Liyanarachchi S, Choi C, Caligiuri MA, et al. BAALC, a novel marker of human hematopoietic progenitor cells. Exp Hematol 2003;31:1051–6.
26. Perry SS, Zhao Y, Nie L, Cochrane SW, Huang Z, Sun XH. Id1, but not Id3, directs long-term repopulating hematopoietic stem-cell maintenance. Blood 2007;110:2351–60.
27. Gautier EL, Shay T, Miller J, Greter M, Jakubzick C, Ivanov S, et al. Gene-expression profiles and transcriptional regulatory pathways that underlie the identity and diversity of mouse tissue macrophages. Nat Immunol 2012;13:1118–28.
28. Imielinski M, Greulich H, Kaplan B, Araujo L, Amann J, Horn L, et al. Oncogenic and sorafenib-sensitive ARAF mutations in lung adenocarcinoma. J Clin Invest 2014;124:1582–6.
29. Solomon BJ, Mok T, Kim DW, Wu YL, Nakagawa K, Mekhail T, et al. First-line crizotinib versus chemotherapy in ALK-positive lung cancer. N Engl J Med 2014;371:2167–77.
30. Gadgeel SM, Gandhi L, Riely GJ, Chiappori AA, West HL, Azada MC, et al. Safety and activity of alectinib against systemic disease and brain metastases in patients with crizotinib-resistant ALK-rearranged non–small-cell lung cancer (AF-002JG): results from the dose-finding portion of a phase 1/2 study. Lancet Oncol 2014;15:1119–28.
31. Vaishnavi A, Le AT, Doebele RC. TRKing down an old oncogene in a new era of targeted therapy. Cancer Discov 2015;5:25–34.
32. Nelson DS, Quispel W, Badalian-Very G, van Halteren AG, van den Bos C, Bovee JV, et al. Somatic activating ARAF mutations in Langerhans cell histiocytosis. Blood 2014;123:3152–5.
33. Hyman DM, Puzanov I, Subbiah V, Faris JE, Chau I, Blay JY, et al. Vemurafenib in multiple nonmelanoma cancers with BRAF V600 mutations. N Engl J Med 2015;373:726–36.
34. Rinehart J, Adjei AA, Lorusso PM, Waterhouse D, Hecht JR, Natale RB, et al. Multicenter phase II study of the oral MEK inhibitor, CI-1040, in patients with advanced non-small-cell lung, breast, colon, and pancreatic cancer. J Clin Oncol 2004;22:4456–62.

35. Haura EB, Ricart AD, Larson TG, Stella PJ, Bazhenova L, Miller VA, et al. A phase II study of PD-0325901, an oral MEK inhibitor, in previously treated patients with advanced non-small cell lung cancer. Clin Cancer Res 2010;16:2450–7.
36. Kirkwood JM, Bastholt L, Robert C, Sosman J, Larkin J, Hersey P, et al. Phase II, open-label, randomized trial of the MEK1/2 inhibitor selumetinib as monotherapy versus temozolomide in patients with advanced melanoma. Clin Cancer Res 2012;18:555–67.
37. Berger MF, Hodis E, Heffernan TP, Deribe YL, Lawrence MS, Protopopov A, et al. Melanoma genome sequencing reveals frequent PREX2 mutations. Nature 2012;485:502–6.
38. Imielinski M, Berger AH, Hammerman PS, Hernandez B, Pugh TJ, Hodis E, et al. Mapping the hallmarks of lung adenocarcinoma with massively parallel sequencing. Cell 2012;150:1107–20.
39. Cancer Genome Atlas Research N. Comprehensive genomic characterization of squamous cell lung cancers. Nature 2012;489:519–25.
40. Zhang J, Ding L, Holmfeldt L, Wu G, Heatley SL, Payne-Turner D, et al. The genetic basis of early T-cell precursor acute lymphoblastic leukaemia. Nature 2012;481:157–63.
41. Gruber TA, Larson Gedman A, Zhang J, Koss CS, Marada S, Ta HQ, et al. An Inv(16)(p13.3q24.3)-encoded CBFA2T3-GLIS2 fusion protein defines an aggressive subtype of pediatric acute megakaryoblastic leukemia. Cancer Cell 2012;22:683–97.
42. Trapnell C, Hendrickson DG, Sauvageau M, Goff L, Rinn JL, Pachter L. Differential analysis of gene regulation at transcript resolution with RNA-seq. Nat Biotechnol 2013;31:46–53.
43. Trapnell C, Williams BA, Pertea G, Mortazavi A, Kwan G, van Baren MJ, et al. Transcript assembly and quantification by RNA-Seq reveals unannotated transcripts and isoform switching during cell differentiation. Nat Biotechnol 2010;28:511–5.
44. Subramanian A, Tamayo P, Mootha VK, Mukherjee S, Ebert BL, Gillette MA, et al. Gene set enrichment analysis: a knowledge-based approach for interpreting genome-wide expression profiles. Proc Natl Acad Sci U S A 2005;102:15545–50.
45. Cheng DT, Mitchell TN, Zehir A, Shah RH, Benayed R, Syed A, et al. Memorial Sloan Kettering–integrated mutation profiling of actionable cancer targets (MSK-IMPACT): a hybridization capture-based next-generation sequencing clinical assay for solid tumor molecular oncology. J Mol Diagn 2015;17:251–64.
46. Frampton GM, Fichtenholtz A, Otto GA, Wang K, Downing SR, He J, et al. Development and validation of a clinical cancer genomic profiling test based on massively parallel DNA sequencing. Nat Biotechnol 2013;31:1023–31.
47. McKerrell T, Park N, Moreno T, Grove CS, Ponstingl H, Stephens J, et al. Leukemia-associated somatic mutations drive distinct patterns of age-related clonal hemopoiesis. Cell Rep 2015;10:1239–45.